Journal of Power Sources 228 (2013) 57–67

Contents lists available at SciVerse ScienceDirect

Journal of Power Sources

journal homepage: www.elsevier.com/locate/jpowsour

Influence of the ionomer type in direct methanol fuel cell (DMFC) anode catalyst layers on the properties of primary and secondary pores

K. Wippermann [a,*], R. Elze [a], C. Wannek [a], H. Echsler [a], D. Stolten [a,b]

[a] Institute of Energy and Climate Research (IEK-3: Fuel Cells), Forschungszentrum Jülich GmbH, 52425 Jülich, Germany
[b] Chair for Fuel Cells, RWTH Aachen University, Germany

HIGHLIGHTS

- Influence of type of ionomer on structure/properties of DMFC anodes.
- Fumion® has a mean tortuosity about twice as high as Nafion®.
- Fumion® ionomers have a stronger tendency to form ionomer films.
- Lower ECSA and lower amount of primary pores in presence of Fumion® ionomers.

ARTICLE INFO

Article history:
Received 4 October 2012
Received in revised form
19 November 2012
Accepted 20 November 2012
Available online 28 November 2012

Keywords:
DMFC anode catalyst layer
Hydrocarbon ionomer
Proton conductivity
Impedance spectroscopy
Primary/secondary pores
Pore size distribution

ABSTRACT

The influence of the ionomer type in DMFC anode catalyst layers (ACLs) on the properties of primary and secondary pores was investigated. Two hydrocarbon ionomers, Fumion®SO-340 and Fumion®S-360, were compared with Nafion®. Electrochemical properties of MEAs and ACLs were determined by galvanostatic *U*/*i*-characteristics, methanol stripping and impedance spectroscopy. Structural properties and chemical compositions of the ACLs were determined by SEM/EDS and automated standard porosimetry. Substitution of Nafion® by hydrocarbon ionomers causes a decrease of maximum power density and active surface area by up to 48% and 91%. Ionomer phases formed by Fumion® ionomers have a mean tortuosity twice as high as Nafion® ionomer phases. The relative percentage of primary pore volume decreases in the order: Nafion® > Fumion®SO-340 > Fumion®S-360, indicating an increased blocking of primary pores by Fumion® ionomer films. The proton conductivities of the primary pores are a factor of 2–5 higher than those of the secondary pores. The results are explained by an enhanced film-forming ability of Fumion® ionomers compared to that of Nafion®, leading to a higher tortuosity of the ionomer phase. By encapsulating primary pores, Fumion® ionomer films block active sites and reduce the active surface and the performance of ACLs and MEAs.

1. Introduction

In order to improve the performance and durability of direct methanol fuel cells (DMFCs) in single cells and fuel cell systems [1] and to reduce the loading of expensive noble metal catalysts, a deeper understanding of the structure–activity relationship of the DMFC catalyst layers is essential. These catalyst layers (CL) usually consist of a carbon supported catalyst, e.g. Pt/C for the cathode and Pt–Ru/C for the anode, and a proton conducting perfluorosulfonic acid ionomer like Nafion®. The proton conducting paths thus generated extend (and significantly enhance) the electrochemical active surface area (ECSA) from the membrane surface into the depth of the catalyst layers. Additionally, the ionomer acts as a binder for the carbon supported catalyst and improves the contact between membrane and catalyst layers. The morphology of the ionomer phase greatly influences the microstructure and properties of the catalyst layers. This primarily concerns the following issues: (i) the electrochemical active surface area (ECSA) respectively the triple phase boundary (TPB), (ii) the pore size distribution and porosity, (iii) the proton transport via the ionomer phase, (iv) the electron transport via the catalyst/carbon phase, (v) the ionomer/catalyst interface represented e.g. by a charge transfer resistance and a double layer capacitance and (vi) the fluid transport in the porous system (methanol, water, CO_2 and air).

Nafion® is the state-of-the-art ionomer serving as proton exchange membrane (PEM) and as proton conducting material in catalyst layers. In order to reduce the water and methanol crossover from the anode to the cathode side of the DMFC, novel membrane

* Corresponding author. Tel.: +49 2461 61 2572; fax: +49 2461 61 6695.
E-mail address: k.wippermann@fz-juelich.de (K. Wippermann).

0378-7753/$ – see front matter © 2012 Elsevier B.V. All rights reserved.
http://dx.doi.org/10.1016/j.jpowsour.2012.11.069

materials have to be developed [2]. However, in terms of electrochemical performance and MEA durability, it is necessary to adapt the electrode design and the membrane/electrode interface to the properties of novel PEM materials. This includes a replacement of Nafion® (equivalent weight (EW) of sulfonic acid groups: 1.11 g mol^{-1}) in the catalyst layers by a novel ionomer. In this study, sulfonated poly(phenylene sulfones) are investigated as anode catalyst ionomers. Two different types of the so-called Fumion® ionomers are used: Fumion® S-360 containing merely sulfone units (−SO_2−) connecting the phenyl rings (EW = 0.36 g mol^{-1}) and Fumion® SO-340 containing sulfone units and ether units (−O−) connecting phenyl rings (EW = 0.34 g mol^{-1}), see Fig. 1. Fumion® S-360 has been introduced into the anode catalyst layers with the same ionomer weight fraction as in conventional Nafion®-based ACLs, whereas the loading of Fumion® SO-340 was lower. Moreover, these novel materials exhibit high thermal, oxidative and hydrolytic stabilities and high proton conductivity (compared to Nafion® a factor of 1.7 higher at same conditions [3]) due to high density of sulfonic acid groups. Because the substitution of Nafion® by sulfonated poly(phenylene sulfones) will most probably change the properties of catalyst layers, a detailed study of the issues raised above is required.

Concerning issue (i), the ECSA has been reported to vary in dependence of type and content of ionomer [4,5]. Regarding issue (ii), the catalyst layer pores may be classified in “primary” and “secondary” pores (Watanabe et al. [6]). Following this classification, primary pores are the smaller pores inside catalyst agglomerates, whereas secondary pores are the larger pores outside or between the agglomerates. From mercury intrusion porosimetry, Watanabe et al. [6] deduced pore diameters of about 50–60 nm for the primary pores and about 0.2–6 μm for the secondary pores. Primary pore sizes up to 100 nm and secondary pore sizes up to 1 μm can be found in the literature [7–11]. Ushida et al. [7] adopted the primary/secondary pore model of Watanabe et al. [6] and raised the problem of poor wetting of primary pores by ionomers (polymers). Tominaka et al. [12] were the first to present an impedance analysis on DMFC catalyst layers based on primary and secondary pores. Their complex equivalent circuit is derived from a transmission line model [13] and includes a secondary pore fraction of reaction sites, θ, which allows to distinguish between the impedance of primary and secondary pores in catalyst layers. It means, that proton and electron conductivities of both primary and secondary pores can be calculated (see issues (iii) and (iv)).

This work deals with the influence of the ionomer type and amount in DMFC anode catalyst layers (ACLs) on the DMFC performance, the active surface of the ACL and the impedance and microstructure of primary and secondary pores. In this context, MEAs without ionomer in the ACL, with Nafion in technically relevant quantities and with alternative sulfonated polysulfone ionomers in two different weight fractions in the ACL have been prepared and studied.

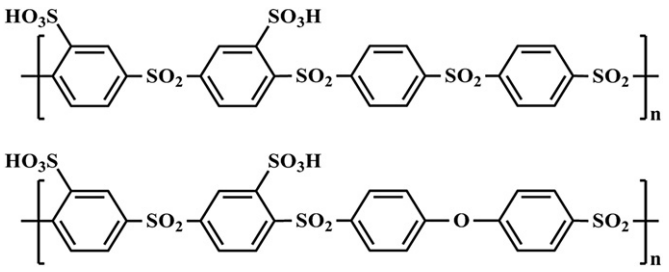

Fig. 1. Fumion® S-360: the aromatic ring bearing the sulfonic acid group is connected to two sulfone linkages (left), Fumion SO-340®: the aromatic ring bearing the sulfonic acid group is connected to a sulfone and an ether linkage (right) [3].

2. Experimental

2.1. MEA preparation

Gas diffusion layers (GDL) were produced in-house by hydrophobizing a commercial carbon cloth and coating it with a microporous layer (containing carbon black and PTFE) by means of an automated doctor blade technique.

For the fabrication of anode catalyst layers dispersions of carbon supported Pt–Ru catalyst (HiSpec 12100 from Johnson Matthey), ionomer solutions (Nafion® dispersion LQ1115 from Ion Power, Fumion® SO-340 and Fumion® S-360 from FuMA-Tech GmbH, St. Ingbert/Germany) and dispersants were prepared by ultrasonic agitation. The homogenized inks were coated onto the in-house GDL by means of doctor blade technique followed by a drying step. The cathodic GDEs were manufactured following the same procedure by using dispersions of carbon supported Pt catalyst (HiSpec 9100 from Johnson Matthey), Nafion® ionomer and dispersants.

The GDEs (anode and cathode) were finished by over-spraying them with Nafion® ionomer solution. The PtRu loading of the anodes was in the range of 2.5–3.3 mg cm^{-2}. The noble metal and ionomer loadings of the anodes are given in Table 1. The table shows a list of the MEAs and GDEs used in this work, including the type of ionomer used for anode preparation, the loading ($m_{\text{ionomer,ACL,PR}}$) and volume ($V_{\text{ionomer,ACL,PR}}$) of the ionomer and the catalyst loading (mgPtRu,ACL) used for preparation and the Nafion® loading ($m_{\text{Nafion®, OS}}$) after overspraying the ACL with Nafion® dispersion. Please note that the ACLs of the GDEs used for porosimetric measurements (ASP) were not oversprayed by Nafion® to allow penetration of octane into the pore system.

The loadings of the cathodes used in this study were: platinum: 2.1 mg cm^{-2}, Nafion® ionomer in the catalyst layer 1.6 mg cm^{-2} and over sprayed Nafion® ionomer 1.1 mg cm^{-2}.

The MEAs were assembled by hot-pressing (130 °C, 0.5 kN cm^{-2}) anode and cathode (active area 17.64 cm^2) with a Nafion®115 membrane. Fig. 2 shows a SEM-micrograph of a MEA in cross section, where the numbers indicate the different layers.

2.2. Electrochemical measurements

All the electrochemical experiments were carried out with the MEAs No. 1–4 (see Table 1) at a temperature of 70 °C and ambient pressure.

2.2.1. Polarization curves and methanol stripping (stripping CV)

For either methanol or water supply of the anode, Ismatec ‘BVGE’ or ‘597A’ pumps were used. The flow rate of the cathode feed gas (air, nitrogen or hydrogen) was adjusted by Brooks mass flow controllers (models ‘5850E’ or ‘5850S’). The temperature was set by an in-house temperature controller.

A Kepco ‘BOP 20-10M’ electronic load was used for recording the polarization curves, which were measured galvanostatically at constant volume flows of 1 M aqueous methanol solution (0.21 ml min^{-1} cm^{-2}) and dried air (37 ml min^{-1} cm^{-2}) at ambient pressure.

The stripping experiments were performed using an ‘IM6 Electrochemical Workstation’ of Zahner® Electric Company. The stripping procedure was carried out as follows

(i) OCV, minimization of cathode polarization (t = 10 min): stepwise substitution of air by nitrogen (192 ml min^{-1}) and hydrogen (50 ml min^{-1}).
(ii) potentiostatic control, adsorption of methanol (t = 10 min): $U = U_{\text{anode}} - U_{\text{cathode}} = 0.1$ V

Table 1
List of the characteristic properties of MEAs and GDEs used in this work.

Sample	Ionomer used for the preparation of anodes	$m_{PtRu,ACL}$/ mg cm^{-2}	$m_{ionomer,ACL,PR}$/ mg cm^{-2}	$V_{ionomer,ACL,PR}$[a]/cm^3	$m_{Nafion®,OS}$/ mg cm^{-2}	Applied method(s)
MEA No. 1	–	2.9	–	0	1.0	*U*/*i*, CV, EIS, SEM/EDS
MEA No. 2	Nafion®	2.5	1.2	0.010	1.1	
MEA No. 3	Fumion® SO-340	2.5	0.6	0.006	1.0	
MEA No. 4	Fumion® S-360	2.9	1.4	0.014	1.0	
GDE No. 1	–	3.2	–	0	–	ASP, SEM
GDE No. 2	–	3.2	–	0	–	
GDE No. 3	Nafion®	3.0	1.4	0.012	–	
GDE No. 4	Nafion®	3.0	1.5	0.012	–	
GDE No. 5	Fumion® SO-340	2.9	0.6	0.006	–	
GDE No. 6	Fumion® SO-340	2.8	0.5	0.005	–	
GDE No. 7	Fumion® S-360	3.3	1.5	0.016	–	
GDE No. 8	Fumion® S-360	3.0	1.4	0.015	–	

[a] Values calculated with an electrode area of 17.64 cm^2 and densities of 2.1 g cm^{-3} for Nafion® and 1.7 g cm^{-3} for the Fumion® ionomers.

(iii) potentiostatic control, exchange of 1 M MeOH by water (t = 30 min): $U = U_{anode} - U_{cathode}$ = 0.1 V (1 min: V_{H_2O} = 8.7 ml min^{-1}, 29 min: V_{H_2O} = 1.1 ml min^{-1}), methanol and intermediates are washed out of the anode pores and remain almost exclusively on the Pt–Ru catalyst surface as adsorbed species.
(iv) 2 stripping cyclovoltammograms (CVs) in the potential range of U = 0.1–0.8 V, scan rate = 10 mV s^{-1}: adsorbed methanol and intermediates (e.g. CO) are stripped off by oxidation to CO_2.

The charge of the oxidation peaks obtained from the first CVs (see Fig. 6) was analyzed by using the charge integration tool of the THALES Z 2.0 fit software of Zahner® Electric Company. This peak charge is a measure for the electrochemical active surface area (ECSA) of catalyst layers. The peak charges of the second CVs amounted to only 5% of the values of the first CVs. The stripping peak charge of a first stripping peak was determined by calculating a (straight) baseline from the associated second peak.

2.2.2. Electrochemical impedance spectroscopy (EIS)

The impedance spectroscopy was performed with the 'IM6 Electrochemical Workstation' of Zahner® Electric Company, too. The spectra were recorded under OCV conditions with an AC amplitude of ±10 mV in a frequency range of 0.25 Hz to 50 kHz. During the EIS measurements the DMFC cathode was fed by hydrogen (V_{H_2} = 50 ml min^{-1}) instead of air and the anode was purged by water (V_{H_2O} = 1.1 ml min^{-1}) instead of 1 M Methanol solution. These operation conditions have been reported to be especially suitable to determine the proton conductivity of the working electrode catalyst layer (here: anode catalyst layer) from – more or less linear – 45° lines obtained in the Nyquist plots at higher frequencies [14–17]. However, with increasing amount of active sites in the primary pores, the 45° slope turns more and more to a semicircle with a 45° slope only at very high frequencies [12], the latter possibly being masked by cable inductances. The exchange current density for the hydrogen oxidation reaction (HOR) is about 4–5 orders of magnitude higher than that of the oxygen reduction reaction (ORR) [18]. Furthermore, our own measurements reveal that the cell impedance under water/hydrogen operation increases by 5 orders of magnitude compared to normal DMFC operation conditions, which is due to a dramatic increase of the anode impedance. Therefore the cathode impedance can be neglected under water/hydrogen operation.

The impedance spectra were fitted by using – among other circuit elements – the porous electrode model proposed by Göhr (see e.g. Ref. [19]) implemented in the THALES Z 2.0 fit software of Zahner® Electric company. The two equivalent circuits used for the fitting procedure with the THALES software are shown in Fig. 3a and b. They are based on a common transmission line model as e.g. proposed by de Levie [13] respectively a more sophisticated transmission line model considering the impedances of primary and secondary pores adapted from the Tominaka model [12] (see Fig. 3c and d). The common transmission line model was used to determine the mean proton resistance as a base value for an estimation of a mean tortuosity exponent of the ionomer phase in the ACL (see Section 3.3, Eq. (3) and Table 3). By means of the complex transmission line model, separate proton resistances of primary and secondary pores could be calculated and compared with the results of porosimetric (ASP) measurements (see Sections 3.3 and 3.4).

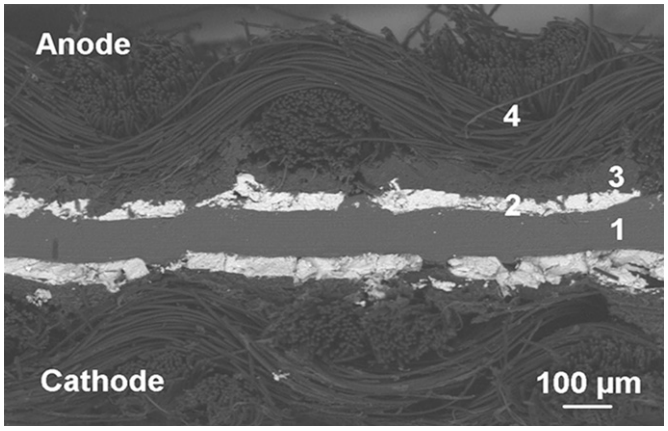

Fig. 2. SEM micrograph of the Fumion® S-360 containing MEA No. 4 in cross section showing the Nafion® membrane (1), the anode catalyst layer (2), the microporous diffusion layer (3) and the carbon cloth substrate (4) (backscattered electrons).

2.3. Automated standard porosimetry (ASP)

The pore size distributions of the GDEs No. 1–8 (see Table 1) were measured by means of an Automated Porosimeter 3.1 Unit by Porotech Ltd. Before starting the experiments, circular samples with a diameter of 23 mm were punched out of the GDEs. Then, the porous samples were heated under vacuum for 1.5 h (T = 170 °C, p = 2 mbar), weighed, cooled down to room temperature, vacuum-filled with octane (p = 2 mbar) and weighed again. For each of the 8 GDEs, 2 circular samples were stacked to exceed the required minimum (octane) liquid mass of about 0.07 g. At a temperature of

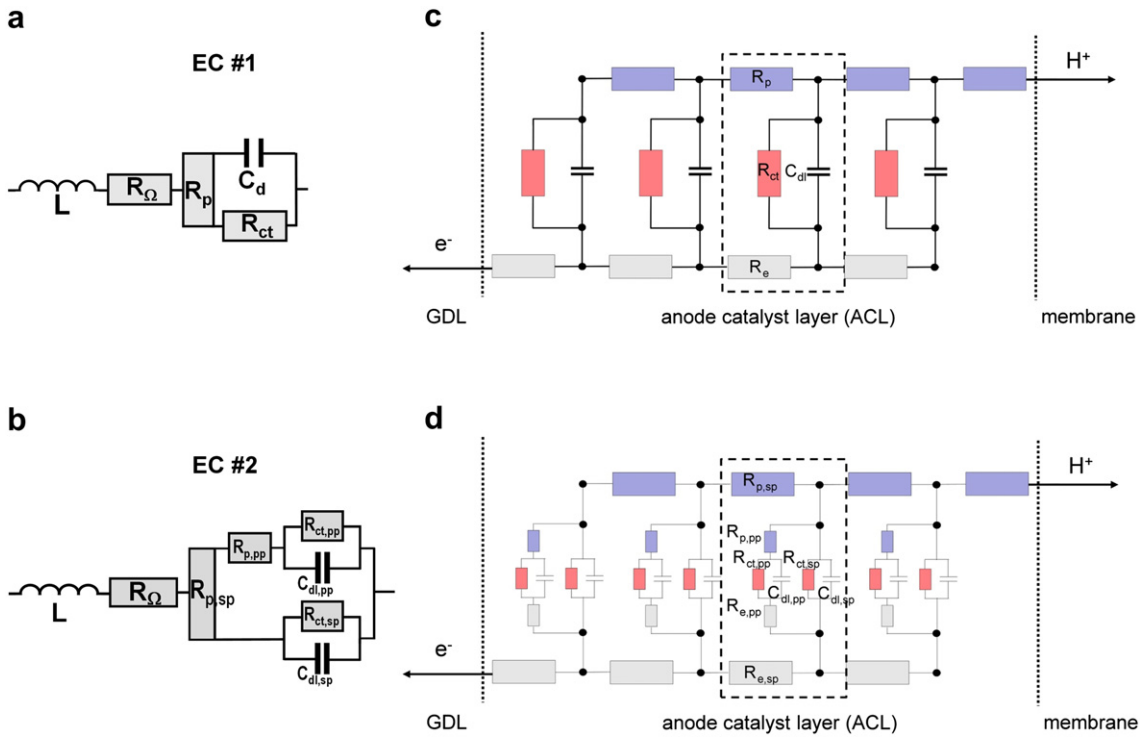

Fig. 3. Equivalent circuits used for the fitting of the impedance spectra with THALES software (a,b) based on transmission line models (c,d); equivalent circuit #2 shown in (b) and (d) considers the impedances of primary and secondary pores and is adapted from the Tominaka model [12]; the rectangles shown with broken lines indicate repeating units within the ACL.

40 °C, the samples were automatically emptied and weighed in a step-by-step process to obtain the pore size distributions (maximum of 100 steps). A more detailed description of the ASP method can be found in Ref. [20].

2.4. SEM/EDS analysis

Cross sections of the MEAs and the GDEs prepared by a scalpel cut were analyzed with a Zeiss Ultra Plus FEG scanning electron microscope. The Zeiss Ultra Plus can be operated at an acceleration voltage between 0.2 kV and 30 kV and has a maximum resolution of 0.8 nm at 15 kV. To prevent charging of uncoated specimen, the SEM is equipped with a charge compensation system.

The SEM is equipped with an EDS-System from Oxford Instruments with a liquid nitrogen cooled Si(Li)-detector (30 mm^2) with a resolution of 127 eV for MN Kα and an INCA Energy 350 software package.

3. Results and discussion

3.1. Microscopic investigations

Fig. 4 shows a SEM-micrograph of the anode catalyst layer of GDE No. 7 in top view. This GDE was prepared for ASP measurements. Here, secondary pores with diameters in the range of some ten nm to several hundred nm are visible as indicated by the arrows.

As described in the Experimental section, the GDEs respectively the catalyst layers were impregnated by overspraying them with Nafion® dispersion prior to the hot-pressing step to improve the contact between the catalyst layers and the membrane. The question that arises is to know which part of the over-sprayed Nafion® penetrates into the pore system of the anode catalyst layer. This question can be answered by using the EDS quantification of fluorine in the anode catalyst layers of the MEAs.

Table 2 gives the fluorine content of the chemical composition in wt% of the MEA anode catalyst layers measured by EDS in cross section after the electrochemical testing. Based on the fluorine contents and the assumption of a fluorine mass fraction in Nafion® polymer of 69%, mass percentages and loadings of Nafion® in the ACL, $m_{Nafion®ACL}$, can be calculated (see Table 2). By subtracting the known Nafion® loading from the MEA preparation, the additional

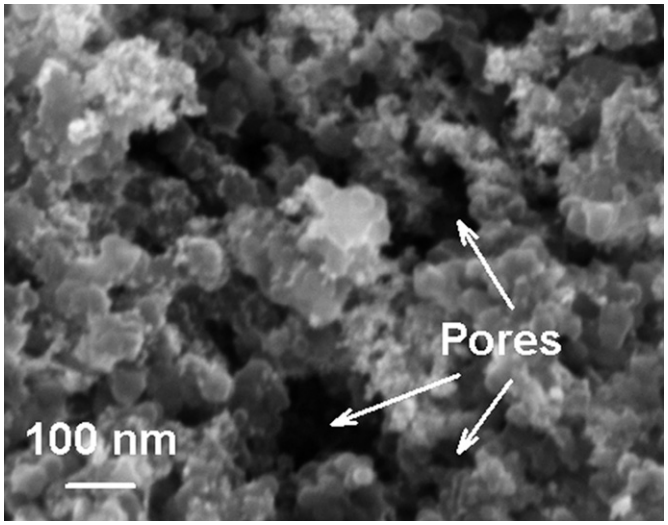

Fig. 4. Micrograph of the Fumion® S-360 containing GDE No. 7 showing secondary pores with diameters of several tenth of nm up to around 100–200 nm, (top view, secondary electrons).

Nafion® loading caused by over-spraying, $m_{\text{Nafion}^{®},\text{ ACL, OS}}$, is obtained (see Table 2). Finally, by adding the known ionomer (Nafion or hydrocarbon) loading during MEA preparation, $m_{\text{ionomer ACL,PR}}$, the total ionomer loading of the ACL, $m_{\text{ionomer ACL}}$, is obtained (see Table 2). It can be seen, that the Fumion®-containing MEAs have the highest (2.1 mg cm^{-2}, S-360) and lowest (1.0 mg cm^{-2}, SO-340) ionomer contents, which are mainly due to the different ionomer loadings during preparation. The uptake of over-sprayed Nafion® (see $m_{\text{Nafion}^{®},\text{ ACL, OS}}$) increases in the order: Nafion® ~ Fumion® SO-340 < Fumion® S-360 < without ionomer.

3.2. Single cell performance and active surface

The performance characteristics of MEAs No. 1–4 prepared with different ionomers in the anode catalyst layers at a temperature of 70 °C are shown in Fig. 5. As can be seen, the power density decreases in the order: Nafion® > without ionomer > Fumion® SO-340 > Fumion® S-360. It is notable, that the sample 'without ionomer' reaches a maximum power density of 97 W cm^{-2}, which is 94% of the value obtained with Nafion® (103 mW cm^{-2} = 100%). This result can be explained by a relatively strong Nafion® filling of the catalyst layer after the spray treatment with Nafion® dispersion, as proven by the SEM/EDS measurements (see above, Section 3.1). In contrast, the MEAs with Fumion® ionomers yield only 78% (Fumion® SO-340, present in the ACL with half of the weight loading compared to the Nafion content of MEA 2) respectively 52% (Fumion® S-360, roughly the same ionomer weight loading as in the Nafion®-based MEA 2) of the maximum power density of the MEA prepared with Nafion®.

Although the slopes of the *U*/*i*-curves of the MEAs prepared with Fumion® ionomers seem to be slightly steeper than that of the MEA with the ACL prepared with Nafion®, the main performance loss in presence of Fumion® ionomer is obviously caused by higher activation overpotentials at low current densities. The latter effect can be due to both loss of ECSA and/or loss of specific activity of the catalyst.

In order to check the ECSA of the anode catalyst layers of the MEAs No. 1–4, methanol stripping experiments (see e.g. Refs. [21–23]) were carried out (for details see Experimental section). The stripping voltammograms are shown in Fig. 6. It should be noted, that the stripping current is normalized to the Pt–Ru loading. This is necessary, because the somewhat different Pt–Ru loadings of the anode catalyst layers have to be taken into account (see Table 1): it can be assumed, that in the loading range of about 2.5–3.0 mg cm^{-2}, the catalyst surface and thus the stripping charge increase linearly with catalyst loading. The linear approach is justified, because the adsorbed methanol and its intermediates (preferentially CO) are oxidized and stripped *throughout* the catalyst layer. As can be seen from Fig. 4, the stripping charge normalized to the Pt–Ru loading, which is a measure for the ECSA, decreases in the same order as observed for the performance (see above). The normalized stripping charges dramatically decrease in presence of the Fumion® ionomers and amount to only 53% (Fumion® SO-340) and 9% (Fumion® S-360) of the value achieved with Nafion®. Simultaneously, the stripping peak potential shifts to

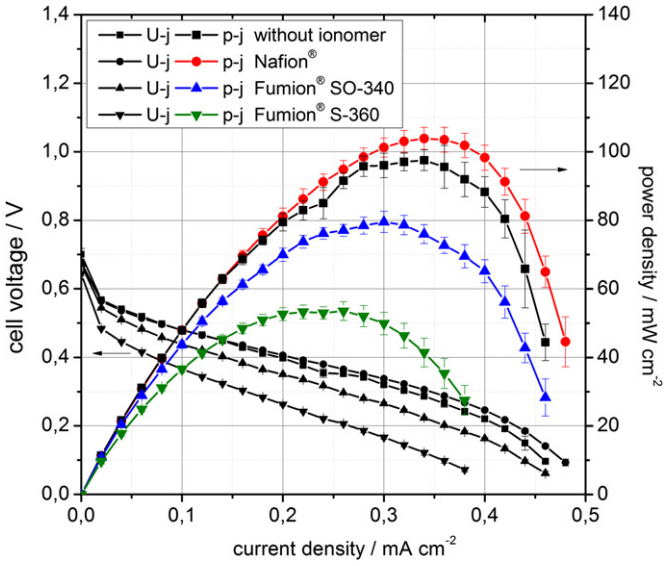

Fig. 5. Performance characteristics of MEAs No. 1–4 prepared with different ionomers in the anode catalyst layers: without ionomer (■), Nafion® (●), Fumion® SO-340 (▲), Fumion® S-360 (▼); T = 70 °C, 1 M aqueous methanol solution (0.21 ml min^{-1} cm^{-2}) and dried air (37 ml min^{-1} cm^{-2}), ambient pressure; errors indicated by bars. PtRu loading of the anodes: 2.5 mg cm^{-2} (■), 2.9 mg cm^{-2} (●), 2.9 mg cm^{-2} (▲), 2.5 mg cm^{-2} (▼); Pt loading of the cathodes: 2.1 mg cm^{-2}.

higher values, indicating a lower specific activity of the catalyst surface especially for the MEA prepared with Fumion® S-360. On the assumption that the Pt–Ru catalyst does not change its catalytic properties during the preparation process, a decrease of the specific activity of the catalyst may be explained with an inhibiting effect of ionomer molecules on the catalyst surface. According to this hypothesis, Fumion® S-360 should have the highest inhibiting effect on methanol oxidation, although it cannot be ruled out that the difference between the samples containing Fumion® SO-340 and Fumion® S-360 is mainly due to a loading effect (cf. Table 1). However, it is not possible to draw a definite conclusion concerning the inhibition mechanism: for example, ionomer molecules in contact with Pt–Ru or even adsorbed on the catalyst surface could influence the electronic properties of the catalyst surface. Secondly, they could reduce the coverage of methanol, intermediates of methanol oxidation and water molecules and thus decrease the reaction rate by a simple blocking mechanism. The latter effect does not necessarily mean that a blocking ionomer film covers the whole catalyst surface. It may also be that catalyst agglomerates are enclosed by an ionomer film which hinders the transport of educts and products to/from the small primary pores and reduces the surface coverage of educts and intermediates on the Pt–Ru particles inside the agglomerate. Such a 'film formation' effect would not only explain a significant decrease of active surface: because the ionomer film covers Pt–Ru particles on the outer surface of the agglomerates, a blocking of active sites and/or a change of the electronic properties of the catalyst may cause a decrease of the specific activity.

Table 2
Nafion and overall ionomer content of the ACLs of MEAs No. 1–4.

MEA No.	Ionomer	$m'_{\text{fluorine ACL}}$ (EDS)[a]/wt%	$m'_{\text{Nafion®ACL}}$/ wt%	$m_{\text{Nafion®ACL}}$/ mg cm^{-2}	$m_{\text{Nafion®,ACL,PR}}$/ mg cm^{-2}	$m_{\text{Nafion®,ACL,OS}}$/ mg cm^{-2}	$m_{\text{ionomer ACL,PR}}$/ mg cm^{-2}	$m_{\text{ionomer ACL}}$/ mg cm^{-2}
1	–	14.8	21.5	1.0	0.0	1.0	0.0	1.0
2	Nafion®	24.0	34.8	1.6	1.2	0.4	1.2	1.6
3	Fumion® SO-340	7.7	11.1	0.4	0.0	0.4	0.6	1.0
4	Fumion® S-360	10.2	14.8	0.7	0.0	0.7	1.4	2.1

[a] Relative deviation of the composition: ±3% for x > 1 wt%.

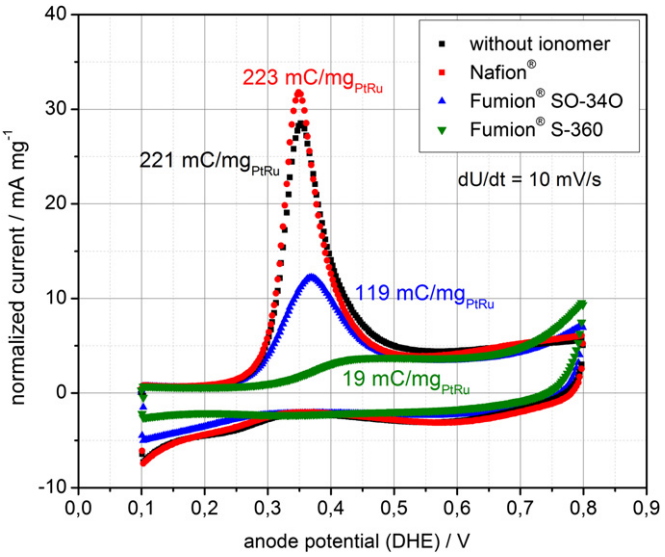

Fig. 6. Methanol stripping of the anode catalyst layers of MEAs No. 1–4 prepared with different ionomers in the anode catalyst layers: without ionomer (■), Nafion® (●), Fumion® SO-340 (▲), Fumion® S-360 (▼); T = 70 °C, anode: V_{H_2O} = 1.1 ml min^{-1}, cathode: V_{H_2} = 50 ml min^{-1}; scan rate: 10 mV s^{-1}; normalized peak charges indicated. PtRu loading of the anodes: 2.5–2.9 mg cm^{-2}.

Fig. 7 exhibits an almost linear connection between the power density and the normalized stripping charge in a broad current range. It means that the influence of the different ionomers on the ECSA of the anode catalyst layers plays an important role in the MEA performance. The increase of the slope almost proportional to the current density is easy to understand: The roughly parallel U/i-characteristics (see Fig. 5) mean a more or less constant difference ΔU in a wide current range and thus an approximately linear increase of ΔP with increasing current density.

It should be mentioned that in contrast to the stripping charge, the power density in this diagram is not directly related to the Pt–Ru loading, because there is no simple linear relationship between the MEA performance and the catalyst loading. This is due to the limited penetration depth of the electrochemical current, which extends from the membrane surface into the catalyst layer and

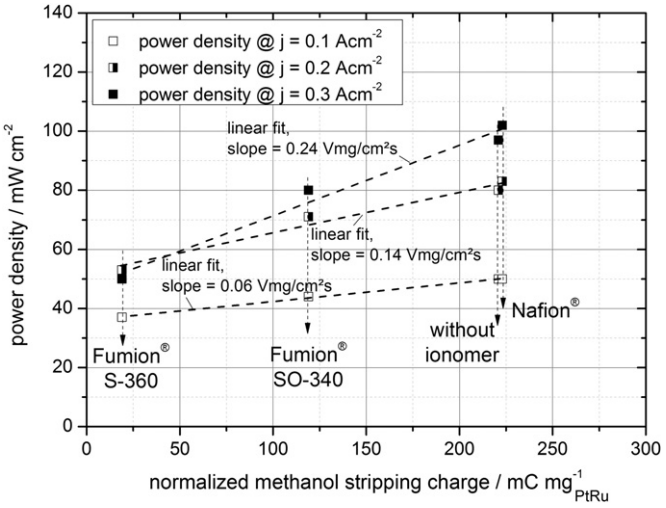

Fig. 7. Correlation of power density and normalized stripping charge at three selected current densities: 0.1 A cm^{-2} (□), 0.2 A cm^{-2} (◨), 0.3 A cm^{-2} (■); PtRu loading of the anodes: 2.5–2.9 mg cm^{-2}; data taken from Figs. 5 and 6.

which decreases with increasing current density [14,24,25]. Therefore, an increased thickness of catalyst layer caused by a higher Pt–Ru loading does not provide a proportional increase of performance.

At an operation temperature of 70 °C, methanol dehydrogenation occurs preferentially at three neighboring Pt sites (see e.g. Ref. [21]). If the number of reaction sites per unit mass of Pt involved in the stripping procedure is expressed in terms of m^2 active surface per gram of Pt, estimated values of the ECSA can be obtained [21]. In our case, the ECSA decreases in the order: 81 m^2 g^{-1} (Nafion) ≈ 80 m^2 g^{-1} (without ionomer) > 43 m^2 g^{-1} (Fumion SO-340) > 7 m^2 g^{-1} (Fumion S-360), corresponding to the normalized charge values shown in Figs. 6 and 7.

3.3. Impedance spectroscopy

Electrochemical impedance spectra were recorded to determine the proton resistance of primary and secondary pores in the anode catalyst layer. Because of the water/hydrogen operation (see Experimental part), the Nyquist plots obtained with the MEAs No. 1–4 shown in Fig. 8 represent mainly the impedance of the anode, the membrane and interfacial contacts.

In accordance with literature [14–17], the spectra can be described to essentially consist of three parts depending on the frequency range: (i) $f \geq 4$ kHz: cable inductance, (ii) 4 kHz > $f \geq$ 50 Hz: 45° line to the real axis, which is dominated by the proton conductivity of the anode catalyst layer, (iii) $f <$ 50 Hz: approximately capacitive behavior corresponding with the double layer capacitance. As described in the Experimental section, the spectra were analyzed on basis of two transmission line models. In Fig. 8, fits based on equivalent circuit (EC) #2 are shown as examples. The small diagram in Fig. 8 demonstrates the superior fitting quality with EC #2 compared to EC #1. As shown in Fig. 3a/b, the equivalent circuits used for the fitting procedure comprise a cable inductance, L, an ohmic resistance, R_Ω, a proton resistance, R_p, a charge transfer resistance, R_{ct}, and a double layer capacitance, C_{dl}. The resistance of electronic conductivity, R_e, does not have to be considered, because R_e is about 3 orders of magnitude lower than R_p [14]. In case of the more complex transmission line model EC #2 taking into account the impedances of primary and secondary

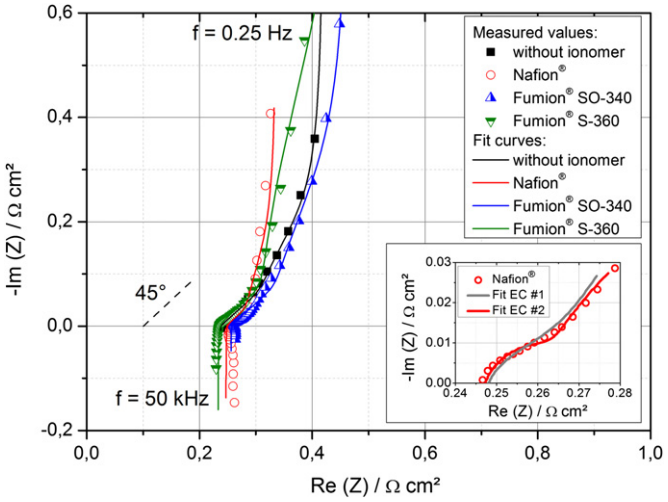

Fig. 8. Nyquist plots of impedance spectra obtained with the MEAs No. 1–4: without ionomer (■), Nafion® (●), Fumion® SO-340 (▲), Fumion® S-360 (▼); T = 70 °C, anode: V_{H_2O} = 1.1 ml min^{-1}, cathode: V_{H_2} = 50 ml min^{-1}; colored lines indicate fit results based on equivalent circuit shown here (see also Fig. 3b); frequency range: 0.25 Hz to 50 kHz; small diagram: comparison of fits with both equivalent circuits.

pores (Fig. 3b/d), R_p, R_{ct} and C_{dl} values were calculated for both primary pores (subscript 'pp') and secondary pores (subscript 'sp'). Because of the predominantly capacitive behavior at low frequencies, the use of charge transfer resistances is not absolutely necessary but improves the fitting quality.

The fitting results obtained from the fit curves in Fig. 8 for the ohmic resistance as well as the proton resistances for primary and secondary pores are shown in the bar diagram of Fig. 9. The resistance values and the percentage value of fitting errors (numbers in brackets) are indicated at the top of the bars. The ohmic resistance, R_Ω, consists basically of the membrane resistance and the interface contact resistances between the membrane and the catalyst layers. Because the membrane and the cathode were virtually identical for all the MEAs investigated, the membrane resistance and the contact resistance between the membrane and the cathode catalyst layer should also be identical. As seen from Fig. 9, R_Ω, is nearly independent on the ionomer used for the preparation of the anode catalyst layers. Hence, the contact resistance between the membrane and the anode catalyst layer is independent on the used ionomer, too. This result can be explained by the spray impregnation of all the GDEs by Nafion® dispersion before the hot-pressing procedure, which provides a good contact between the Nafion® membrane and the catalyst layers (see Section 2.1).

The R_p values of the primary pores are a factor of 2–5 higher than those of the secondary pores (see Fig. 9). One explanation might be the film-forming properties of the ionomers: Because of the high tortuosity of these films (see below), the connectivity between the proton conducting paths in the primary pores and secondary pores may be poor, leading to high proton resistances. Because the MEA 'without ionomer' (MEA No. 1) is nevertheless impregnated by Nafion® dispersion, its R_p values have the same order of magnitude as compared to the other samples. The overall ionomer loading of the anode catalyst layer of the 'Nafion®' sample (MEA No. 2) is however higher than that of MEA No. 1 (see Table 2), which explains the lower R_p values of MEA No. 2 (see Fig. 9).

More difficult to understand are the higher R_p values of MEAs No. 3 and 4 (Fumion® ionomers) compared to MEA No. 2 as the overall ionomer content (from ACL preparation and spray treatment) of these MEAs is nearly as high as in MEA 2 (case of MEA No. 3 with SO-340) or even by 50% higher (MEA No. 4 with S-360, see last column of Table 2). Furthermore, the specific conductivity of both Fumion® ionomers is about a factor of 1.7 higher than that of Nafion® [3].

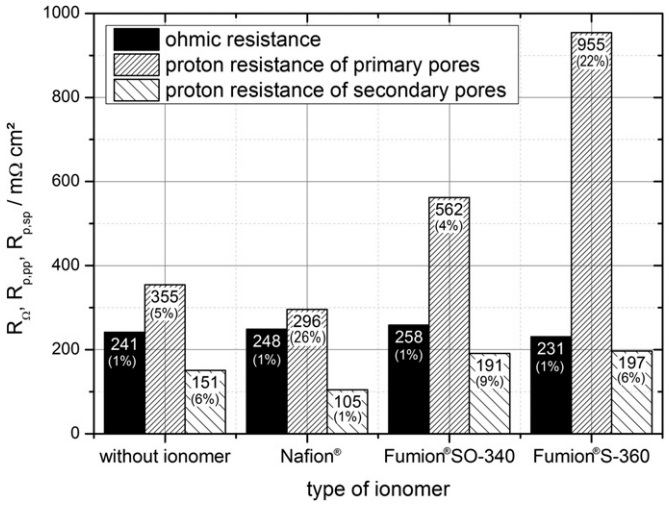

Fig. 9. Fitting results for the ohmic resistance and the proton resistances for primary and secondary pores of the MEAs No. 1–4; data obtained from the fit curves shown in Fig. 8; resistance values and percentage value of fitting errors (numbers in brackets) indicated at the top of the bars.

In order to explain this result, we first need to consider the factors which determine the proton resistance. R_p essentially depends on the following properties of the ionomer phase in the catalyst layer: (i) volume fraction, (ii) tortuosity, (iii) connectivity and (iv) specific conductivity. Points (ii) and (iii) require further clarification: According to literature, the tortuosity of gas-diffusion media like catalyst layers can be defined as the ratio of the actual path length for the transport of a species (gases, liquids, protons, electrons) through the porous layer and the layer thickness [26]. The actual path length is always higher than the layer thickness because of merging, branching, and curving of pores [27]. It should be noted, that the tortuosity values estimated in our work are mean values. A more sophisticated analysis including synchrotron tomography and 3D simulations according to a multi-layer model leads to a probability distribution of tortuosity [28].

The higher the volume fraction, the connectivity and the specific conductivity and the lower the tortuosity, the lower is the proton resistance. The specific proton conductivity of the anode catalyst layer (ACL) is calculated according to Eq. (1), with $R_{p,ACL}$ as proton resistance of the ACL, d_{ACL} as mean thickness of the ACL and A_{ACL} as the geometric area of the electrode ($A_{ACL} = 17.64\ cm^2$):

$$\sigma_{p,\,ACL} = \frac{d_{ACL}}{A_{ACL} * R_{p,\,ACL}} \tag{1}$$

According to Refs. [14,29], the specific proton conductivity of the anode catalyst layer is correlated with the specific proton conductivity of the ionomer by the following empirical equation,

$$\sigma_{p,\,ACL} = \varepsilon^{n_{p,\,ACL}} * \sigma_{ionomer} \tag{2a}$$

with ε as volume fraction of the ionomer phase in the ACL (e.g. $\varepsilon = 0.1$ at 10 vol% ionomer) and the tortuosity exponent $n_{p,ACL}$ of the ionomer phase in the ACL. Rearrangement of Eq. (2a) yields:

$$n_{p,\,ACL} = \frac{\ln\left(\frac{\sigma_{p,\,ACL}}{\sigma_{ionomer}}\right)}{\ln \varepsilon} \tag{2b}$$

The exponent $n_{p,ACL}$ is of particular interest, because it reflects the tortuosity of the ionomer phase. In case of the MEAs No. 3 and 4, two different ionomers are present in the anode catalyst layer. It is, however, not possible to differentiate between the proton resistances of the ionomer phases (Fumion®/Nafion®) in the anode catalyst layer. This is because the R_p values obtained from impedance spectroscopy reflect a mean resistance of both ionomers, resulting in mean specific proton conductivities, $\overline{\sigma}_{p,\,ACL}$, of the anode catalyst layers. Nevertheless, a mean tortuosity exponent, $\overline{n}_{p,ACL}$, can be calculated according to Eq. (3),

$$\overline{n}_{p,\,ACL} = \frac{\ln\left(\frac{\overline{\sigma}_{p,\,ACL}}{\overline{\sigma}_{ionomer}}\right)}{\ln \varepsilon_{ACL}} \tag{3}$$

where the volume fraction of ionomer, ε_{ACL}, is given by the following equation:

$$\varepsilon_{ACL} = \frac{V_{ionomer\ ACL,\ PR} + V_{Nafion^{®}\ ACL,\ OS}}{V_{ACL}} = \frac{V_{ionomer\ ACL}}{V_{ACL}} \tag{4}$$

The volumes of the ionomer phases are calculated from the known mass fractions and densities of the ionomers ($\rho = 2.1\ g\ cm^{-3}$ for Nafion® and 1.7 g cm^{-3} for the Fumion® ionomers).

The mean specific conductivity $\overline{\sigma}_{\text{ionomer}}$, is calculated from the specific conductivities and the relative volume fractions of the ionomer used for preparation and over-sprayed Nafion penetrated in the ACL:

$$\overline{\sigma}_{\text{ionomer ACL}} = \sigma_{\text{ionomer ACL, PR}} * \varepsilon_{\text{ionomer ACL, PR}} + \sigma_{\text{Nafion® ACL, OS}} * \varepsilon_{\text{Nafion® ACL, OS}} \quad (5)$$

Please note, that the volume fractions, $\varepsilon_{\text{ionomer ACL,PR}}$ and $\varepsilon_{\text{Nafion®, ACL, OS}}$, refer to the volume of the ionomer phase, not to the volume of the total anode catalyst layer. The specific conductivities of the ionomers were estimated by interpolation from literature data, considering fully humidified conditions ($\sigma_{\text{Nafion® EW1100}} \approx 0.10$ S cm^{-1} [30–32], $\sigma_{\text{Fumion® SO-340}} \approx \sigma_{\text{Fumion® S-360}} \approx 0.17$ S cm^{-1} [3]). It should be mentioned, that the specific conductivities of Nafion® membranes to be found in the literature differ from about 0.08 to 0.12 S cm^{-1} under comparable operation conditions.

Because the ionomer phases in the primary and secondary pores are connected in a complex way, i.e. in series as well as in parallel, Eq. (3) cannot be simply adapted to calculate separate tortuosity exponents for the primary and secondary pores. In order to still obtain an estimate of the mean tortuosity exponent, $\overline{n}_{\text{p, ACL}}$, a mean proton resistance, $\overline{R}_{\text{p, ACL}}$, should be used instead. $\overline{R}_{\text{p, ACL}}$ equals the R_{p} value obtained from the impedance spectra of MEAs No. 1–4 by using the simplified equivalent circuit shown in Fig. 3a/c.

The physical and geometrical parameters of the ACLs of MEAs No. 1–4 are shown in Table 3. The volume of the ionomer in ACL due to preparation, $V_{\text{ionomer ACL,PR}}$, and volume of Nafion® in ACL due to over-spraying, $V_{\text{Nafion®, ACL, OS}}$, were calculated by multiplying $m_{\text{ionomer ACL,PR}}$ and $m_{\text{Nafion®, ACL, OS}}$ (see Table 2) by the geometric area of the anode (17.64 cm^2) and dividing these values by the densities of the corresponding ionomers (Nafion®: $\rho = 2.1$ g cm^{-3}, Fumion®: 1.7 g cm^{-3}). The volume fraction of ionomer in ACL due to preparation, $\varepsilon_{\text{ionomer ACL,PR}}$, and the volume fraction of Nafion® in ACL due to over-spraying, $\varepsilon_{\text{Nafion®, ACL, OS}}$, were calculated as dimensionless fractions using the sum of $V_{\text{ionomer ACL,PR}}$ and $V_{\text{Nafion®, ACL, OS}}$ as the normalizing value. The mean thickness of ACL, d_{ACL}, was obtained from microscopic examination of MEA cross sections. The volume of ACL, V_{ACL}, was obtained by multiplying d_{ACL} with the area of 17.64 cm^2. The volume fraction of ionomer in ACL, ε_{ACL}, was calculated by Eq. (4). The mean proton resistance in ACL, $\overline{R}_{\text{p, ACL}}$, was taken from the R_{p} value obtained from the fitting of the impedance spectra (EC #1). The mean specific proton conductivity of ACL, $\overline{\sigma}_{\text{p, ACL}}$, was calculated in an analogous way to Eq. (1) and the mean specific proton conductivity of the ionomer phase in ACL, $\overline{\sigma}_{\text{ionomer ACL}}$, was calculated by Eq. (5). Finally, the mean tortuosity of the proton conducting paths in primary and secondary pores $\overline{n}_{\text{p, ACL}}$, was calculated by Eq. (3).

The low tortuosity exponent of the latter ones of around 1 is unexpected, because a non-tortuosity of the Nafion® phase is improbable. A similar tortuosity exponent, or *vice versa*, a too high specific conductivity of the porous layer, has also been found by Boyer et al. [29]. They interpreted this result by an additional proton conducting mechanism via anion impurities on the carbon surface. Our own measurements revealed that in case of ACLs with unsupported catalysts (Pt–Ru black) and Nafion®, where proton conducting carbon is missing, higher tortuosity exponents of 1.7–2.0 are obtained [14]. These findings suggest that the tortuosity exponents calculated on basis of Eq. (3) are underestimated. It can however be assumed that this underestimation applies equally to all the ACLs studied in this work. Bearing in mind this fact, the mean tortuosity exponents of the ACLs containing hydrocarbon ionomers, especially that of Fumion® S-360, are significantly higher than compared to the $\overline{n}_{\text{p, ACL}}$ values of ACLs containing only Nafion® (MEAs No. 1 and 2). Fumion® ionomer phases having a pronouncedly higher tortuosity than Nafion® explain the higher R_{p} values of MEAs No. 3 and 4 (Fumion® ionomers) compared to MEA No. 1. This result is in accordance with the assumption of enhanced film-forming properties of Fumion® ionomers, as argued from the results of the stripping voltammograms (see Section 3.2, Fig. 6).

3.4. Automated standard porosimetry (ASP)

To gain a better understanding of the different R_{p} values of primary and secondary pores, more information about the microstructure, i.e. pore size distribution of the ACLs is necessary. Unfortunately, the pore size distribution of self-standing catalyst layers is hardly to determine. This is not only due to preparation issues: in order to obtain valid results, a minimum liquid mass of 0.07 g is mandatory which corresponds to a minimum specimen thickness of 300–500 μm, depending on the porosity and the liquid (e.g. octane or water). As free-standing CLs cannot be prepared and characterized, we decided to measure the pore size distributions of complete GDEs prepared with nominally the same catalyst layers as in the MEAs No. 1–4 and to accept the overlap of pore size distributions of ACL, micro layer and carbon cloth. It should be mentioned, that the GDEs used for the ASP measurements were not over-sprayed by Nafion® (see also Table 1). This is because only a fraction of the over-sprayed Nafion® penetrates into the ACL, the rest forms a film on the surface of the porous sample, which complicates and delays the establishment of a capillary equilibrium.

Fig. 10a/b shows the differential pore size distribution of four selected GDEs. Additionally, the classification result of the pore volumes for all the samples measured are summarized in Table 4.

Fig. 10a exhibits three sharp pore size maxima at ~80 nm, ~2.5 μm and ~14 μm. The maximum around ~80 nm can be attributed to secondary pores in both the anode catalyst layer and the micro layer, whereas the maxima in the μm range match the size of cracks in the aforementioned layers as well as large pores/voids in the carbon cloth (see Figs. 2 and 4). Thus, the large pores beyond 1 μm diameter can neither be associated with primary pores nor with secondary pores in the ACL. They will therefore not be considered in the following discussion. This is in accordance

Table 3
Physical and geometrical parameters of the ACLs of MEAs No.1–4.

MEA No.	Ionomer	$V_{\text{ionomerACL,PR}}$/ cm^3	$V_{\text{Nafion® ACL,OS}}$/cm^3	$\varepsilon_{\text{ionomer ACL, PR}}$/–	$\varepsilon_{\text{Nafion® ACL,OS}}$/–	d_{ACL}/ μm	V_{ACL}/ cm^3	ε_{ACL}/ –	$\overline{R}_{\text{p, ACL}}$/ Ω cm^2	$\overline{\sigma}_{\text{p, ACL}}$/ S cm^{-1}	$\overline{\sigma}_{\text{ionomer}}$/ S cm^{-1}	$\overline{n}_{\text{p, ACL}}$/–
1	–	0	0.0086	0	1	37	0.065	0.13	0.26	0.014	0.10	1.0
2	Nafion®	0.0102	0.0031	0.77	0.23	35	0.062	0.22	0.20	0.017	0.10	1.1
3	Fumion® SO-340	0.0061	0.0036	0.63	0.37	34	0.060	0.16	0.31	0.011	0.13	1.4
4	Fumion® S-360	0.0143	0.0057	0.72	0.28	43	0.076	0.26	0.28	0.015	0.16	1.8

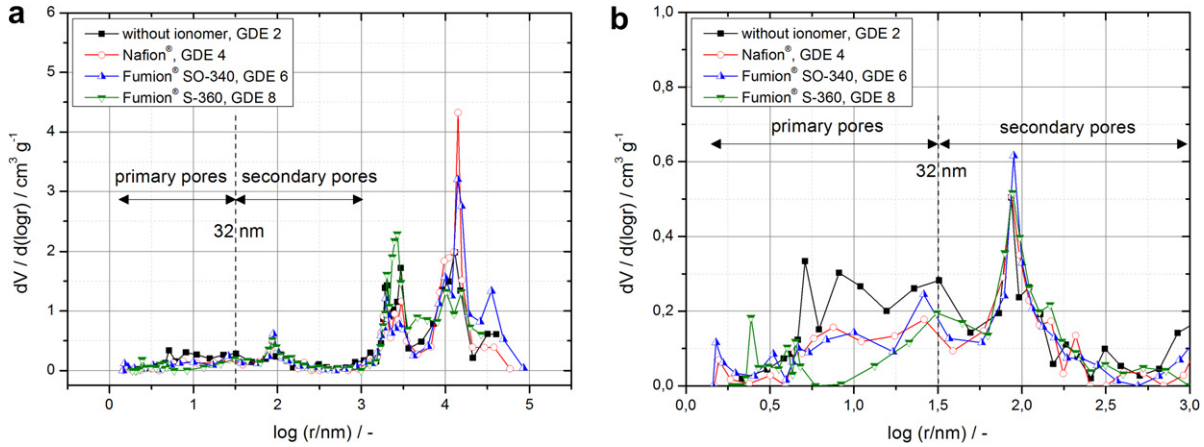

Fig. 10. Differential pore size distribution of four selected GDEs prepared with different ionomers in the anode catalyst layers: without ionomer (■), Nafion® (●), Fumion® SO-340 (▲), Fumion® S-360 (▼); automated standard porosimetry working conditions: $T = 40$ °C, $p = 1$ bar ($r < 10$ nm: p = 2 mbar); (a) complete pore size distribution, (b) pore size range of primary and secondary pores.

with literature [7–11], where the upper limit of secondary pore size has been found to be 1 μm [7,8] or even lower [9–11].

The maxima in the pore size range of less than log $r = 1.5$ ($r = 32$ nm) are not very distinct (see Fig. 10b). This is however – apart from the irrelevant region at $r > 1$ μm – the pore size range, where the various ionomers in the ACLs cause the largest difference in the differential pore size distribution. Following the assumption of enhanced film-forming properties of the Fumion® ionomers which was raised above, a 'covering' of catalyst agglomerates by an ionomer film should especially influence the pore size distribution of the primary pores. To the aforementioned reasons, the small pores with a diameter <32 nm (log(r/nm) = 1.5) can, in particular, be associated with primary pores. Hence, a pore diameter of around 30 nm is estimated as an approximate limit between primary and secondary pores, a value which lies in the middle of the range of 10–100 nm reported in the literature [7–11]. It should be noted, that in the pore size range up to 1 μm, there is an overlap of the pore volumes of the ACLs and micro layers (the latter formed by carbon and PTFE particles). Therefore, the pore size distributions of the micro layers – which nominally should be identical for all the GDEs investigated – have a 'dampening' effect on the influence of the ionomers on the primary and secondary pore size distributions of the ACLs.

As shown in Table 4, by far the highest primary pore volumes are obtained for the GDEs without ionomer, being about twice as large as the values of the other GDEs. This is not astonishing, since the ionomer (Nafion®) content in these samples amounts to zero (compare values of $V_{\text{ionomer,ACL,prep}}$ in Table 1). The decrease of the mean primary pore volume in the order 'without ionomer' > 'Fumion® SO-340' ≈ 'Nafion®' > 'Fumion® S-360' (see Table 4) roughly corresponds to the increase of the ionomer volume, $V_{\text{ionomer,ACL,prep}}$, in the order 'without ionomer' < 'Fumion® SO-340' < 'Nafion®' < 'Fumion® S-360' (see Table 1). However, this

Table 4
Classification of pore volumes of 8 GDEs in the pore size range of $r = 1$ nm to 100 μm (log $r = 0$–5); increments of log $r = 0.5$ as well as categorization in primary pores (log $r < 0.5$) and secondary pores (log $r > 0.5$).

log (r/nm)	ΔV/cm³ g⁻¹							
	Without ionomer		Nafion®		Fumion® SO340		Fumion® S-360	
	GDE No. 1	GDE No. 2	GDE No. 3	GDE No. 4	GDE No. 5	GDE No. 6	GDE No. 7	GDE No. 8
0–0.5	0.03	0.02	0.01	0.01	0.02	0.01	0.00	0.01
0.5–1	0.08	0.09	0.03	0.04	0.01	0.04	0.04	0.01
1–1.5	0.16	0.11	0.08	0.08	0.07	0.08	0.08	0.03
1.5–2	0.10	0.11	0.09	0.08	0.12	0.09	0.09	0.11
2–2.5	0.06	0.06	0.07	0.07	0.07	0.07	0.04	0.08
2.5–3	0.03	0.04	0.02	0.01	0.03	0.02	0.01	0.02
3–3.5	0.27	0.34	0.24	0.27	0.25	0.23	0.24	0.42
3.5–4	0.27	0.23	0.26	0.23	0.24	0.25	0.19	0.38
4–4.5	0.53	0.49	0.71	0.63	0.60	0.74	0.53	0.48
4.5–5	0.13	0.13	0.00	0.09	0.32	0.25	0.28	0.00
0–5	1.64	1.63	1.51	1.50	1.74	1.77	1.48	1.56
Average value	1.63		1.50		1.75		1.52	
<1.5 (Primary pores)	0.26	0.22	0.12	0.13	0.11	0.13	0.11	0.06
Average value	0.24		0.12		0.12		0.09	
%[a]	55		42		38		33	
1.5–3 (Secondary pores)	0.18	0.21	0.18	0.16	0.21	0.17	0.14	0.22
Average value	0.20		0.17		0.19		0.18	
%[a]	45		58		62		67	

[a] Percentage value related to the total volume of primary and secondary pores.

order needs to be qualified by stating that the difference of the individual results for the primary pore volume of the two quasi-identical GDEs prepared with Fumion® S-360 is higher than the difference between the mean primary pore volumes obtained for the GDEs prepared with Fumion® S-360 and Fumion® SO-340/Nafion®. Because the ionomer volume in the 'Nafion' GDEs (Nos. 3a and 4) is about twice as high as that in the 'Fumion® SO-340' GDEs (Nos.5a and 6), one would expect a significantly higher (primary) pore volume for the GDE prepared with Fumion® SO-340 ionomer. However, the primary pore volumes of the GDEs with Fumion® SO-340 and Nafion® are similar. This result is consistent with the idea of an increased 'encapsulation' of primary pores (agglomerates of catalyst) by Fumion® films. Although the lowest primary pore volume of the 'Fumion® S-360' GDEs (mean value of Nos.7a and 8) corresponds to the highest ionomer content as well as enhanced film formation, the difference of primary pore volume between the GDEs Nos. 7a and 8 should be considered (see above). The decrease of the relative percentage of primary pore volume in the order: 'Nafion®' > 'Fumion® SO-340' > 'Fumion® S-360' (and *vice versa* increase of the relative percentage of secondary pores, see Table 4) also supports the idea of enhanced film-forming properties of the Fumion® ionomers. This fits in well with the increase of both the $R_{p,pp}$ values (compare Fig. 9, Section 3.3) and mean tortuosity values (compare Table 3, Section 3.3) in the same order.

The ratio of the highest and lowest values of mean primary pore volume amounts to 2.7. This is similar compared to the corresponding quotients of the values of $R_{p,pp}$ and mean tortuosity (3.2 and 2.1). In contrast, the mean secondary pore volume fluctuates by only about 15% (see Table 4), whereas the quotient of the values of $R_{p,sp}$ amounts to 1.9 (see Fig. 9). These results suggest that the above mentioned 'dampening effect' of the micro layer in the ASP measurements is much stronger in case of the secondary pores. A possible explanation lies in the assumption, that the 'encapsulation' by ionomer films plays a major role for the primary pores, but only a minor role for the − larger − secondary pores. Thus, the 'dampening' effect of the micro layer is weakened in case of the primary pores.

4. Conclusions

The influence of the ionomer on the microstructure and the electrochemical properties of primary and secondary pores in DMFC anode catalyst layers were investigated. It turned out, that ionomer phases formed by Fumion® ionomers (Fumion® SO-340 and Fumion® S-360) have a mean tortuosity about twice as high as Nafion® ionomer phases. The higher tortuosity of the Fumion® ionomers phases may be caused by a stronger tendency to form ionomer films in the catalyst layers. The assumption of enhanced film-forming ability of Fumion® ionomers compared to that of Nafion® is supported by the following results:

(i) the pronounced decrease of the electrochemical active surface area (ECSA) up to 91% (Fumion® S-360), which suggests an ionomer film blocking the catalyst surface and/or hindering the access of primary pores (inside the catalyst agglomerates).
(ii) the proton conductivity values of the primary pores being a factor of 2–5 higher than those of the secondary pores, suggesting a poor connectivity between the tortuous proton conducting paths in the primary and secondary pores.
(iii) the decrease of the relative percentage of primary pore volume/increase of the relative percentage of secondary pores in the order: 'Nafion®' > 'Fumion® SO-340' > 'Fumion® S-360', which indicates an increased blocking of primary pores by Fumion® ionomer films.

The film forming and most probably also the 'encapsulation' properties of the three ionomers used in this work are significantly different. Thus, the type of ionomer has a strong influence on the microstructure and electrochemical properties of the anode catalyst layers. In our future studies, final evidence about the microstructure of the ionomer phases/films could be obtained by TEM measurements (see e.g. Ref. [33]).

Acknowledgments

The authors are grateful to Sina Chirayath for performing the porosimetric measurements and Katja Klafki for the preparation of embedded samples for scanning electron microscopy.

This work was part of a project funded by the German Federal Ministry of Economics and Technology under contract number 0327850.

References

[1] J. Mergel, H. Janssen, M. Müller, J. Wilhelm, D. Stolten, Journal of Fuel Cell Science and Technology 9 (2012). 031011–031010.
[2] C. Wannek, A. Glüsen, D. Stolten, Desalination 250 (2010) 1038–1041.
[3] M. Schuster, K.-D. Kreuer, H.T. Andersen, J. Maier, Macromolecules 40 (2007) 598–607.
[4] J.-H. Kim, H.Y. Ha, I.-H. Oh, S.-A. Hong, H.N. Kim, H.-I. Lee, Electrochimica Acta 50 (2004) 801–806.
[5] S. Sambandam, V. Ramani, Electrochimica Acta 53 (2008) 6328–6336.
[6] M. Watanabe, M. Tomikawa, S. Motoo, Journal of Electroanalytical Chemistry and Interfacial Electrochemistry 195 (1985) 81–93.
[7] M. Uchida, Y. Fukuoka, Y. Sugawara, N. Eda, A. Ohta, Journal of The Electrochemical Society 143 (1996) 2245–2252.
[8] J.-H. Kim, H.Y. Ha, I.-H. Oh, S.-A. Hong, H.-I. Lee, Journal of Power Sources 135 (2004) 29–35.
[9] H.-Y. Jung, K.-Y. Cho, Y.M. Lee, J.-K. Park, J.-H. Choi, Y.-E. Sung, Journal of Power Sources 163 (2007) 952–956.
[10] S. Tominaka, K. Goto, T. Momma, T. Osaka, Journal of Power Sources 192 (2009) 316–323.
[11] Z. Wang, Y. Liu, V.M. Linkov, Journal of Power Sources 160 (2006) 326–333.
[12] S. Tominaka, N. Akiyama, T. Momma, T. Osaka, Journal of The Electrochemical Society 154 (2007) B902–B909.
[13] R. de Levie, Electrochimica Acta 9 (1964) 1231–1245.
[14] A. Havránek, K. Wippermann, Journal of Electroanalytical Chemistry 567 (2004) 305–315.
[15] M. Eikerling, A.A. Kornyshev, Journal of Electroanalytical Chemistry 475 (1999) 107–123.
[16] R. Makharia, M.F. Mathias, D.R. Baker, Journal of The Electrochemical Society 152 (2005) A970–A977.
[17] L. Birry, C. Bock, X. Xue, R. McMillan, B. MacDougall, Journal of Applied Electrochemistry 39 (2009) 347–360.
[18] J. Zhang, Z. Xie, J. Zhang, Y. Tang, C. Song, T. Navessin, Z. Shi, D. Song, H. Wang, D.P. Wilkinson, Z.-S. Liu, S. Holdcroft, Journal of Power Sources 160 (2006) 872–891.
[19] N. Wagner, T. Kaz, K.A. Friedrich, Electrochimica Acta 53 (2008) 7475–7482.
[20] Y.M. Volfkovich, V.S. Bagotzky, V.E. Sosenkin, I.A. Blinov, Colloids and Surfaces A: Physicochemical and Engineering Aspects 187–188 (2001) 349–365.
[21] A.S. Aricò, V. Baglio, A. Di Blasi, E. Modica, P.L. Antonucci, V. Antonucci, Journal of Electroanalytical Chemistry 557 (2003) 167–176.
[22] M. Carmo, V.A. Paganin, J.M. Rosolen, E.R. Gonzalez, Journal of Power Sources 142 (2005) 169–176.
[23] J. Prabhuram, N.N. Krishnan, B. Choi, T.-H. Lim, H.Y. Ha, S.-K. Kim, International Journal of Hydrogen Energy 35 (2010) 6924–6933.
[24] A.A. Kulikovsky, Electrochemistry Communications 5 (2003) 530–538.
[25] A.A. Kulikovsky, Electrochimica Acta 55 (2010) 6391–6401.
[26] M.J. Martinez, S. Shimpalee, J.W. Van Zee, Journal of The Electrochemical Society 156 (2009) B80–B85.
[27] A. Suzuki, U. Sen, T. Hattori, R. Miura, R. Nagumo, H. Tsuboi, N. Hatakeyama, A. Endou, H. Takaba, M.C. Williams, A. Miyamoto, International Journal of Hydrogen Energy 36 (2011) 2221–2229.
[28] G. Gaiselmann, R. Thiedmann, I. Manke, W. Lehnert, V. Schmidt, Computational Materials Science 59 (2012) 75–86.
[29] C. Boyer, S. Gamburzev, O. Velev, S. Srinivasan, A.J. Appleby, Electrochimica Acta 43 (1998) 3703–3709.
[30] F.N. Büchi, G.G. Scherer, Journal of Electroanalytical Chemistry 404 (1996) 37–43.
[31] S. Ochi, O. Kamishima, J. Mizusaki, J. Kawamura, Solid State Ionics 180 (2009) 580–584.
[32] V. Neburchilov, J. Martin, H. Wang, J. Zhang, Journal of Power Sources 169 (2007) 221–238.

[33] J. Xie, F. Xu, D.L. Wood, K.L. More, T.A. Zawodzinski, W.H. Smith, Electrochimica Acta 55 (2010) 7404–7412.

List of symbols

A_{ACL}: geometric area of the anode (17.64 cm^2)/cm^2
C_d: double layer capacitance/F cm^{-2}
$C_{d,pp}$: double layer capacitance of primary pores/Ω cm^2
$C_{d,sp}$: double layer capacitance of secondary pores/Ω cm^2
d_{ACL}: mean thickness of ACL/μm
ε_{ACL}: volume fraction of ionomer in ACL, related to the volume of ACL/−
$\varepsilon_{ionomerACL,PR}$: volume fraction of ionomer in ACL due to preparation, related to the volume of ionomer phase in ACL/−
$\varepsilon_{Nafion^{®}\ ACL,\ OS}$: volume fraction of Nafion in ACL due to over-spraying, related to the volume of ionomer phase in ACL/−
L: cable inductance/H
$m_{ionomer\ ACL}$: total ionomer loading of ACL/mg cm^{-2}
$m_{ionomer\ ACL,PR}$: ionomer loading of ACL due to preparation/mg cm^{-2}
$m'_{fluorine\ ACL}$: fluorine content of ACL obtained from EDS/wt%
$m_{Nafion^{®}\ ACL}$: total Nafion® loading of ACL/mg cm^{-2}
$m'_{Nafion^{®}\ ACL}$: total Nafion® loading of ACL/wt%
$m_{Nafion^{®}\ ACL,\ OS}$: Nafion® loading of ACL due to over-spraying/mg cm^{-2}
$m_{Nafion^{®}\ ACL,\ PR}$: Nafion® loading of ACL due to preparation/mg cm^{-2}
$m_{Nafion^{®},\ OS}$: mass of over-sprayed Nafion®/mg cm^{-2}
$m_{PtRu,ACL}$: PtRu loading of ACL/mg cm^{-2}
$n_{p,ACL}$: tortuosity of the proton conducting paths in ACL/−
$\overline{n}_{p,ACL}$: mean tortuosity of the proton conducting paths in primary and secondary pores of ACL/−
R_{Ω}: ohmic resistance/Ω cm^2
R_p: resistance of proton conductivity/Ω cm^2
$R_{p,pp}$: resistance of proton conductivity in primary pores/Ω cm^2
$R_{p,sp}$: resistance of proton conductivity in secondary pores/Ω cm^2
$R_{p,ACL}$: resistance of proton conductivity in ACL/Ω cm^2
$\overline{R}_{p,\ ACL}$: mean resistance of proton conductivity in primary and secondary pores of ACL/Ω cm^2
r: pore radius/nm
$\sigma_{ionomer}$: specific proton conductivity of an ionomer/S cm^{-1}
$\sigma_{ionomer\ ACL,PR}$: specific proton conductivity of an ionomer in ACL due to preparation/S cm^{-1}
$\overline{\sigma}_{ionomer\ ACL}$: mean specific proton conductivity of the ionomer phase in ACL/S cm^{-1}
$\sigma_{Nafion^{®}\ ACL,\ OS}$: specific proton conductivity of over-sprayed Nafion® in ACL/S cm^{-1}
$\sigma_{Nafion^{®}\ EW1100}$: specific proton conductivity of Nafion® with an equivalent weight of 1100/S cm^{-1}
$\sigma_{p,ACL}$: specific proton conductivity of ACL/S cm^{-1}
$\overline{\sigma}_{p,\ ACL}$: mean specific proton conductivity of ACL/S cm^{-1}
V: pore volume of anode GDE/cm^3 g^{-1}
V_{ACL}: volume of ACL/cm^3
$V_{ionomer\ ACL}$: volume of ionomer in ACL/cm^3
$V_{ionomer\ ACL,PR}$: volume of ionomer in ACL due to preparation/cm^3
$V_{Nafion^{®},\ ACL,\ OS}$: volume of Nafion® in ACL due to over-spraying/cm^3